Supporting Information for

Theoretical prediction of efficient Cu-based dual-atom alloy catalysts for electrocatalytic nitrate reduction to ammonia via high-throughput first-principles calculations

Yuanyuan Wang[a], Chunmei Tang[a,b*], Qianlin Li[a], Ting Xiao[a], Fujian Xiong[a]

a College of Mechanics and Engineering Science, Hohai University, Nanjing 210098, PR China

b National Laboratory of Solid State Microstructures, Nanjing University, Nanjing 210093, PR China

[*]Corresponding author. E-mail: tcmnj@163.com (C. Tang)

Table S1. The zero-point energy corrections (ΔE_{ZPE}) and entropic contributions ($T\Delta S$) (at 298.15 K) to the free energies of the key intermediates

Species	E_{ZPE} (eV)	TS (eV)
*NO_3	0.40	0.27
*NO_3H	0.62	0.27
*NO_2	0.27	0.18
*NO_2H	0.54	0.18
OH+NO_2	0.62	0.27
2*OH+*NO	0.92	0.25
*OH+*NO	0.53	0.20
*OH+*NOH	0.82	0.23
*NO-end	0.18	0.13
*NO-side	0.17	0.11
*NOH	0.45	0.17
*HNO	0.48	0.12
*N	0.08	0.03
*NH	0.38	0.04
*NH_2	0.68	0.09
*NH_3	1.00	0.14
*HNOH	0.77	0.18
*OH+*NH	0.72	0.16
OH+NH_2	1.06	0.15
OH+NH_3	1.37	0.22
*OH	0.34	0.08
2*OH	0.69	0.19
*N_2O_2	0.36	0.23
*N_2O_2H	0.70	0.23
*N_2O	0.26	0.21
*N_2OH	0.56	0.18
*N_2	0.17	0.22

Table S2. The zero-point energy corrections (ΔE_{ZPE}) and entropic contributions ($T\Delta S$) (at 298.15 K) to the free energies of the relevant molecules.

Species	E_{ZPE} (eV)	TS (eV)
HNO_3(g)	0.70	0.83
HNO_2 trans(g)	0.53	0.77
NO_2(g)	0.23	0.74
NO(g)	0.12	0.65
NH_3(g)	0.89	0.60
H_2(g)	0.27	0.40
H_2O(g)	0.56	0.67
N_2(g)	0.15	0.58
N_2O(g)	0.29	0.68

Table S3. The key parameters of the TM_2Cu systems: formation energy (E_{form}) and binding energy (E_b) of the TM_2Cu systems, average net charge (ΔQ) of the TM dimers, distance ($d_{TM\text{-}TM}$) between the embedded TM dimer, distance ($d_{TM\text{-}Cu}$) between the embedded TM atom and its bonded Cu atoms.

TM_2Cu	E_{form} (eV)	E_b (eV)	ΔQ (e)	$d_{TM\text{-}TM}$ (Å)	$d_{TM\text{-}Cu}$ (Å)				
Sc_2Cu	0.94	-11.61	-2.00	2.85	2.66	2.59	2.49	2.59	2.68
Ti_2Cu	0.07	-12.45	-1.51	2.44	2.58	2.59	2.59	2.60	2.58
V_2Cu	**-0.64**	**-11.75**	**-0.79**	**1.81**	2.53	2.71	2.83	2.71	2.53
Cr_2Cu	0.29	-8.87	-0.73	2.68	2.60	2.53	2.49	2.53	2.60
Mn_2Cu	**-0.18**	**-9.14**	**-0.59**	**2.65**	2.56	2.53	2.49	2.53	2.57
Fe_2Cu	**-0.30**	**-11.12**	**-0.29**	**2.28**	2.50	2.57	2.62	2.57	2.50
Co_2Cu	**-0.50**	**-11.51**	**-0.08**	**2.31**	2.49	2.55	2.60	2.55	2.49
Ni_2Cu	0.01	-11.65	0.09	2.52	2.52	2.52	2.52	2.52	2.52
Zn_2Cu	0.10	-5.66	-0.18	2.59	2.55	2.52	2.51	2.53	2.55
Y_2Cu	1.35	-11.48	-1.29	3.12	2.84	2.71	2.57	2.71	2.85
Zr_2Cu	0.43	-14.90	-1.03	2.67	2.67	2.63	2.56	2.63	2.67
Nb_2Cu	**-0.78**	**-15.59**	**-0.62**	**2.29**	2.62	2.65	2.66	2.65	2.61
Mo_2Cu	**-2.11**	**-13.73**	**-0.53**	**1.85**	2.61	2.74	2.85	2.72	2.61
Ru_2Cu	**-0.47**	**-14.97**	**0.09**	**2.36**	2.58	2.57	2.60	2.55	2.56
Rh_2Cu	0.16	-14.25	0.30	2.55	2.58	2.54	2.53	2.53	2.57
Pd_2Cu	0.14	-11.63	0.33	2.63	2.60	2.54	2.51	2.54	2.60
Ag_2Cu	0.09	-8.39	0.11	2.65	2.65	2.58	2.53	2.58	2.65
Cd_2Cu	0.23	-4.59	-0.18	2.78	2.72	2.63	2.58	2.63	2.72
Hf_2Cu	0.56	-15.15	-2.38	2.74	2.63	2.59	2.51	2.59	2.65
Ta_2Cu	**-0.46**	**-17.65**	**-1.20**	**2.42**	2.60	2.62	2.60	2.62	2.60
W_2Cu	**-1.35**	**-15.76**	**-0.55**	**2.26**	2.58	2.62	2.66	2.62	2.58
Re_2Cu	**-1.36**	**-14.67**	**-0.13**	**2.30**	2.58	2.59	2.64	2.58	2.57
Os_2Cu	**-0.81**	**-16.38**	**0.23**	**2.39**	2.57	2.56	2.59	2.55	2.57
Ir_2Cu	0.01	-17.02	0.49	2.52	2.57	2.54	2.54	2.53	2.57
Pt_2Cu	0.19	-13.53	0.58	2.63	2.59	2.54	2.51	2.54	2.59
Au_2Cu	0.19	-10.51	0.43	2.68	2.64	2.56	2.52	2.56	2.63
Cu(111)	--	--	0.02	2.52	2.52	2.52	2.52	2.52	2.52

Table S4. The key parameters of NO_3^- adsorption on the TM_2Cu systems: distance between the O atoms in $*NO_3$ and its bonded TM atoms, d(M-O*); adsorption free energy of NO_3^-, $\Delta G(*NO_3)$; net charge of the $*NO_3$, $\Delta Q(*NO_3)$; net charge of TM dimer with adsorption of NO_3^-, ΔQ(TM-$*NO_3$).

TM_2Cu	d(M-*O) (Å)	$\Delta G(*NO_3)$ (eV)	$\Delta Q(*NO_3)$ (e)	ΔQ(TM-$*NO_3$) (e)
V_2Cu	1.96, 1.96	-1.51	0.87	-0.54
Mn_2Cu	2.00, 1.99	-0.89	0.79	-0.44
Fe_2Cu	1.96, 1.96	-0.89	0.77	-0.50
Co_2Cu	1.96, 1.96	-0.64	0.74	-0.48
Nb_2Cu	2.07, 2.07	-1.07	0.70	-0.54
Mo_2Cu	2.08, 2.08	-1.60	0.87	-0.72
Ru_2Cu	2.10, 2.10	-0.64	0.67	-0.38
Ta_2Cu	2.04, 2.04	-2.06	1.14	-0.88
W_2Cu	2.01, 2.01	-2.21	1.05	-0.96
Re_2Cu	2.05, 2.05	-1.40	0.85	-0.82
Os_2Cu	2.11, 2.11	-0.60	0.69	-0.66
Cu111	2.03, 2.03	0.02	0.70	-0.10

Table S5. The key parameters of H atoms adsorption on the TM_2Cu systems: distance between the H atoms and TM dimers or Cu atoms, Δd(TM/Cu-H*); adsorption free energy of H atoms, ΔG(*H); net charge of the *H, ΔQ(*H); net charge of TM dimer with adsorption of H, ΔQ(TM-*H).

TM_2Cu	Δd(TM/Cu-*H) (Å)	ΔG(*H) (eV)	ΔQ(*H) (e)	ΔQ(TM-*H) (e)
V_2Cu	1.85, 1.86, 1.81	-0.43	0.53	-0.45
Mn_2Cu	1.81, 1.81, 1.77	-0.38	0.49	-0.28
Fe_2Cu	1.73, 1.73, 1.82	-0.44	0.41	-0.26
Co_2Cu	1.69, 1.68, 1.83	-0.47	0.33	-0.19
Nb_2Cu	1.90, 1.90, --	-0.59	0.44	-0.46
Mo_2Cu	1.92, 1.92, --	-0.12	0.46	-0.19
Ru_2Cu	1.82, 1.82, 1.90	-0.34	0.28	-0.18
Ta_2Cu	1.90, 1.90, --	-0.87	0.82	-0.80
W_2Cu	1.86, 1.86, --	-0.58	0.56	-0.59
Re_2Cu	1.90, 1.90, --	-0.40	0.37	-0.33
Os_2Cu	1.82, 182, --	-0.34	0.24	-0.22
Cu111	1.73, 1.73, 1.74	-0.18	0.27	-0.08

Table S6. The calculated values of U_L and corresponding potential-determining step (PDS) for eNO_3RR on TM_2Cu systems.

TM_2Cu	U_L (V)	Limiting step
V_2Cu	-0.73	$*OH+*NH_3 \rightarrow *NH_3$
Mn_2Cu	-0.18	$*NO \rightarrow *NOH$
Fe_2Cu	-0.30	$*NO \rightarrow *NOH$
Co_2Cu	-0.28	$*NO \rightarrow *NOH$
Nb_2Cu	-0.80	$*OH+*NH_3 \rightarrow *NH_3$
Mo_2Cu	-0.76	$*OH+*NH_3 \rightarrow *NH_3$
Ru_2Cu	-0.46	$*NO \rightarrow *NOH$
Ta_2Cu	-1.48	$*OH+*NH_3 \rightarrow *NH_3$
W_2Cu	-1.30	$*OH+*NH_3 \rightarrow *NH_3$
Re_2Cu	-0.78	$*OH+*NH_3 \rightarrow *NH_3$
Os_2Cu	-0.57	$*NO \rightarrow *NOH$
Cu(111)	-0.38	$*NO_2 \rightarrow *NO_2H$

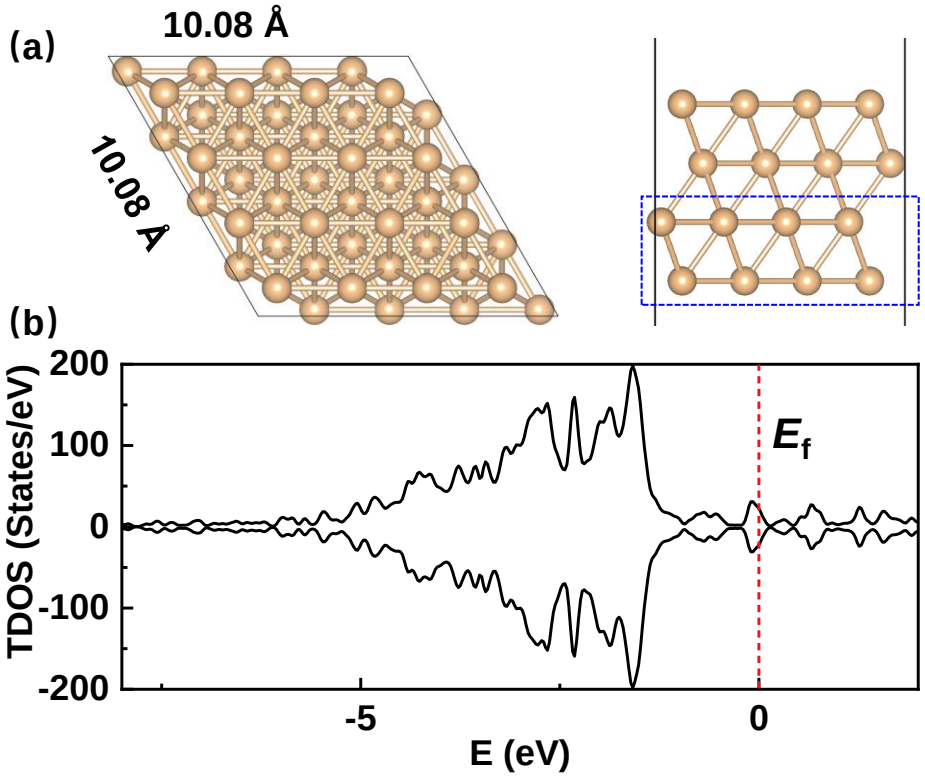

Fig. S1. (a) The atom configurations of 4×4×4 supercell of the pristine Cu(111) slab, with the bottom two layers were fixed. (b) The total densities of states (TDOS) of the pristine Cu(111) slab.

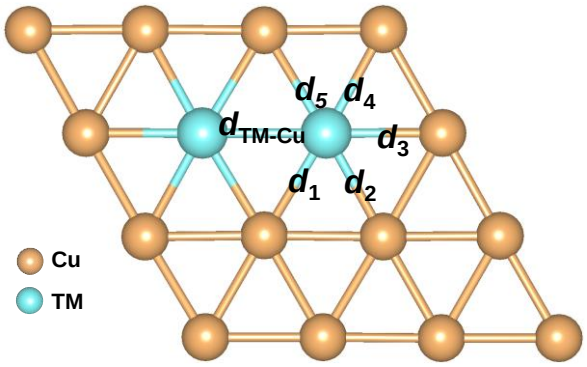

Fig. S2. The sites of TM bonding with Cu atoms, and d_1, d_2, d_3, d_4 and d_5 corresponding to the values of d_{TM-Cu} in Table S3, respectively.

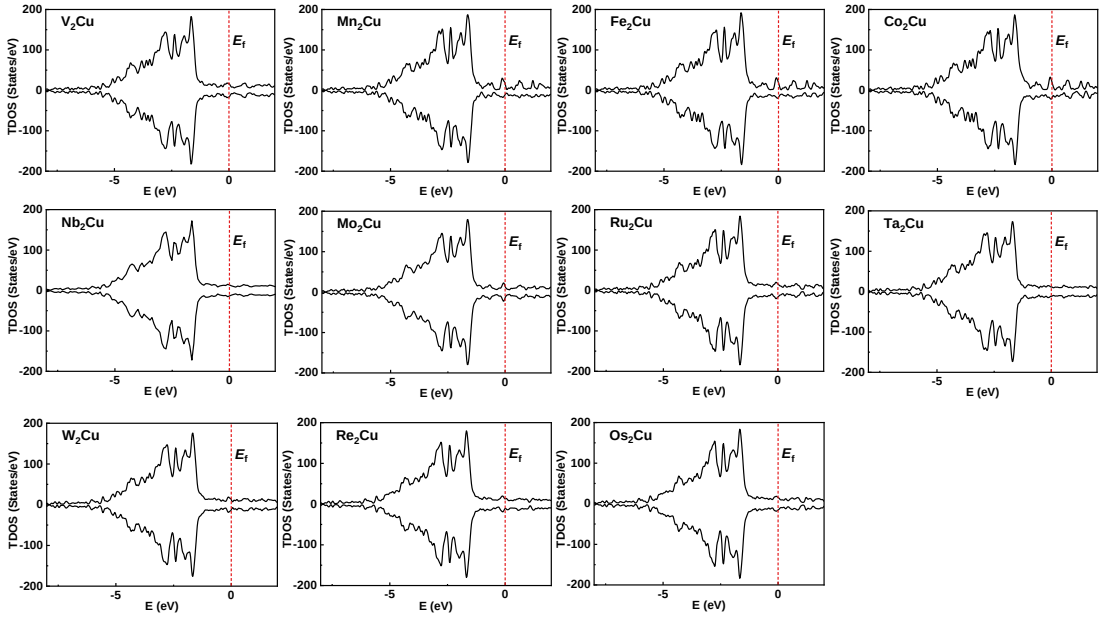

Fig. S3. The total densities of states (TDOS) of the screened TM_2Cu systems.

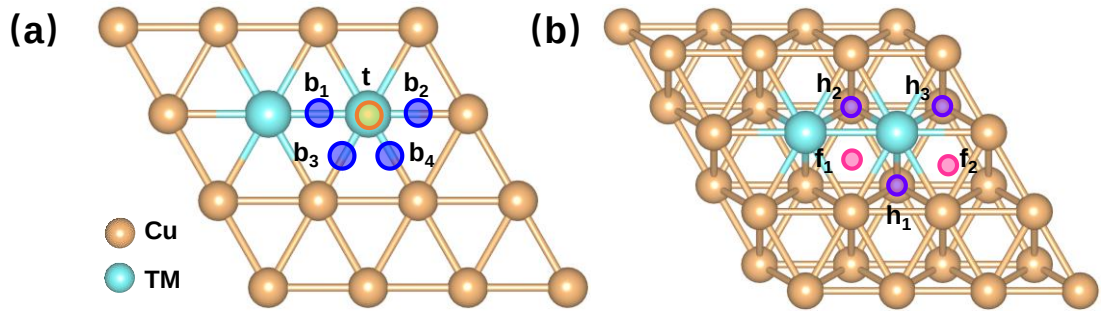

Fig. S4. (a) The considered adsorption sites of NO_3^- adsorbed on screened TM_2Cu catalysts, b_1, b_2, b_3, b_4, and t represent different bridge site and top site respectively. (b) The considered adsorption sites of H atom adsorbed on screened TM_2Cu catalysts, f_1, f_2 and f_3 represent different fcc site, respectively, h_1, h_2 and h_3 represent different hollow site, respectively.

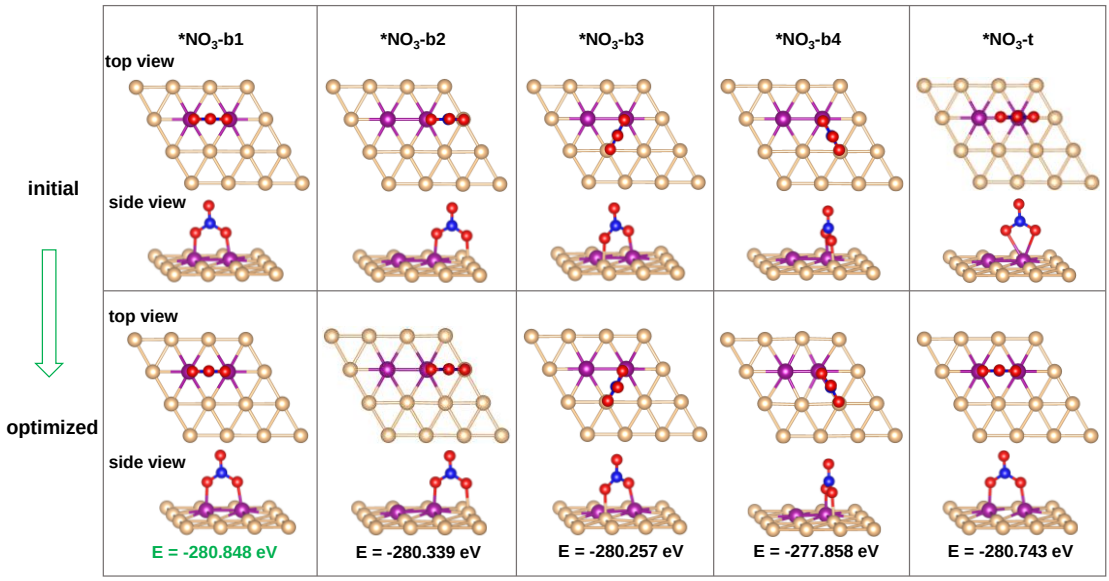

Fig. S5. The initial and optimized structures of several possible NO_3^- adsorption on Mn_2Cu catalyst.

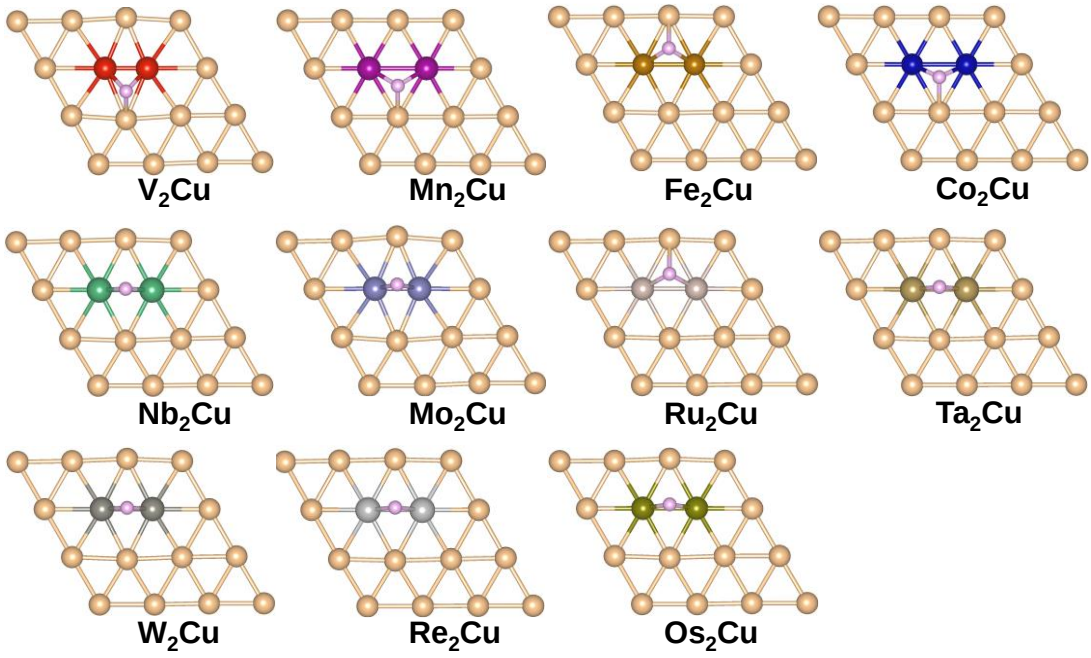

Fig. S6. The most stable adsorption configurations of H atoms on screened TM_2Cu catalysts.

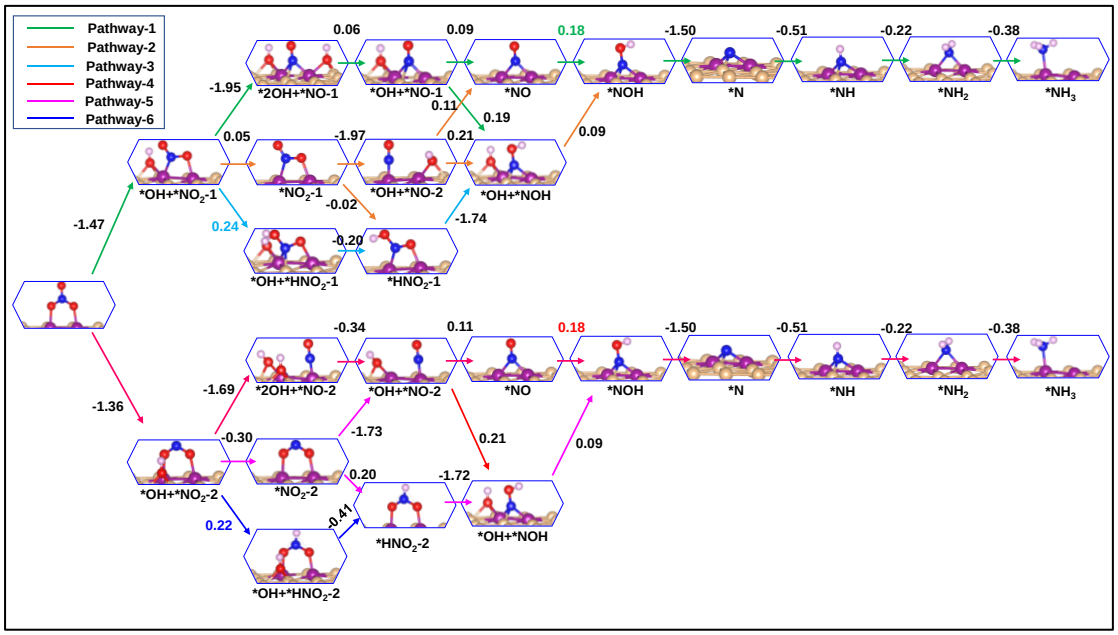

Fig. S7. The all possible reaction pathway on Mn_2Cu catalyst, which contain the optimized reaction intermediate structures and free energy changes in each elementary step. The green pathway contains the most stable configurations of the overall reaction, while the other color pathways along relatively unstable structures.

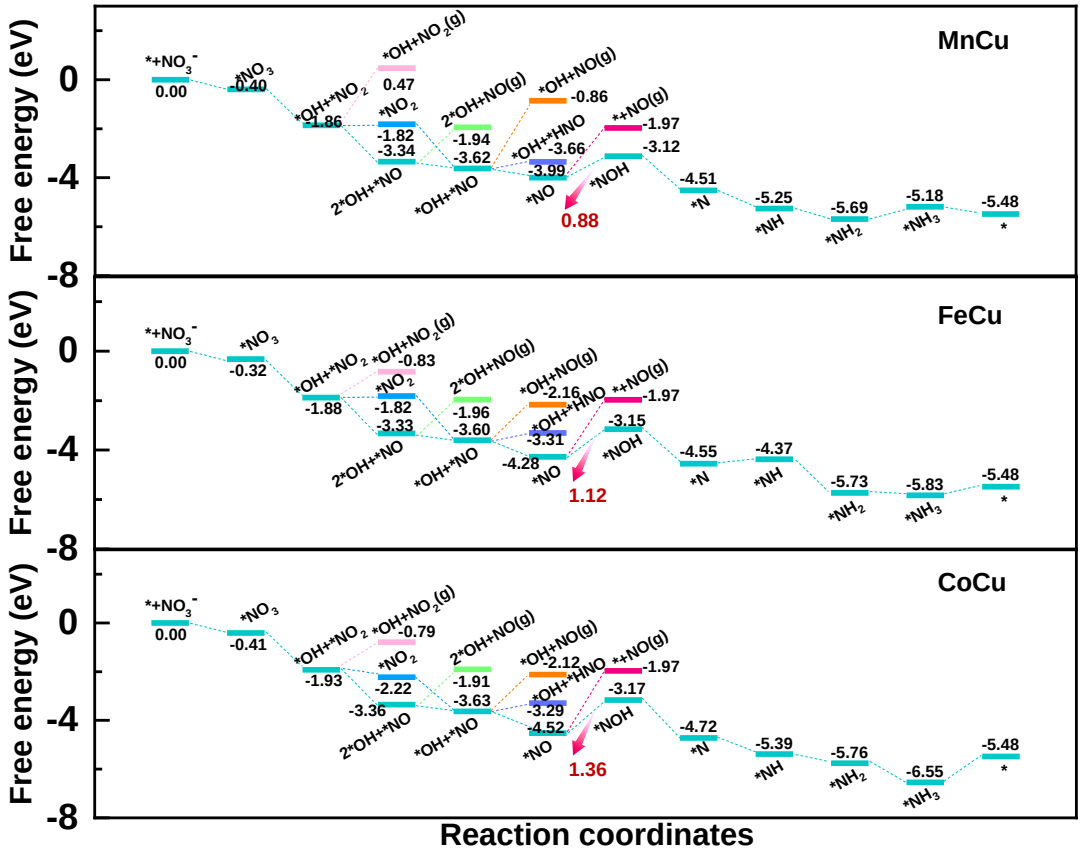

Fig. S8. Free energy diagram and the configurations of corresponding intermediates for the eNO_3RR on MnCu, FeCu, and CoCu SAA catalysts.

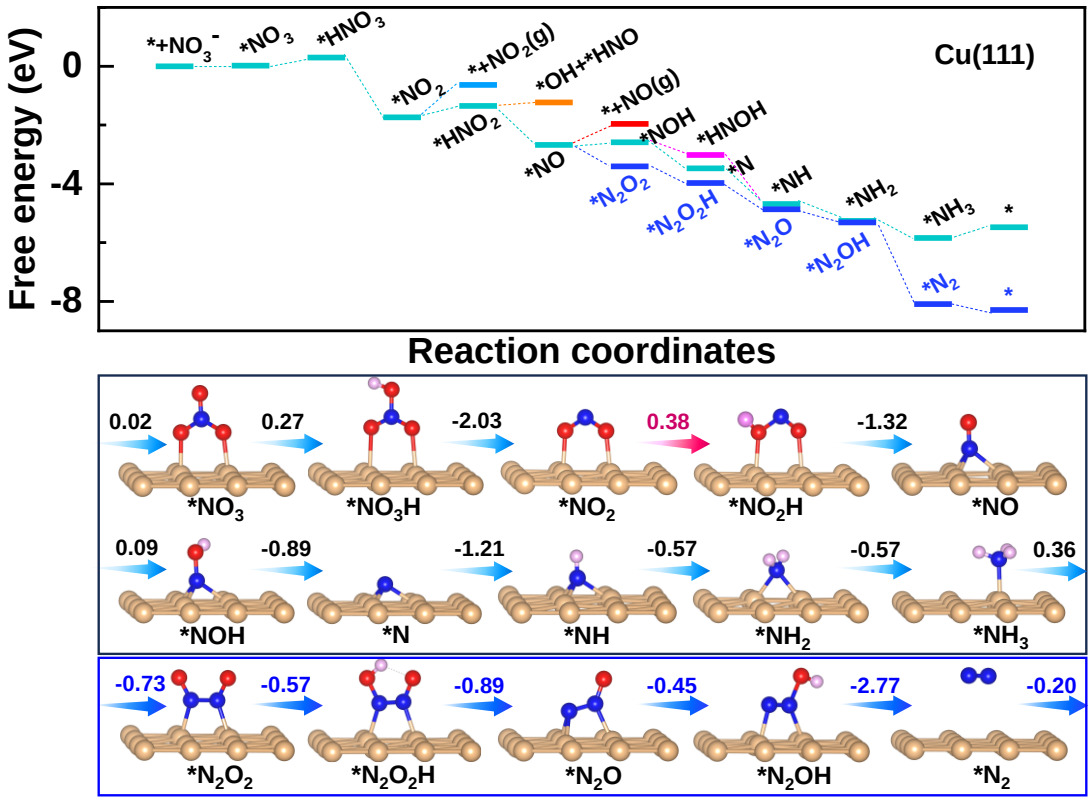

Fig. S9. Free energy diagram and the configurations of corresponding intermediates for the eNO$_3$RR on pristine Cu(111).

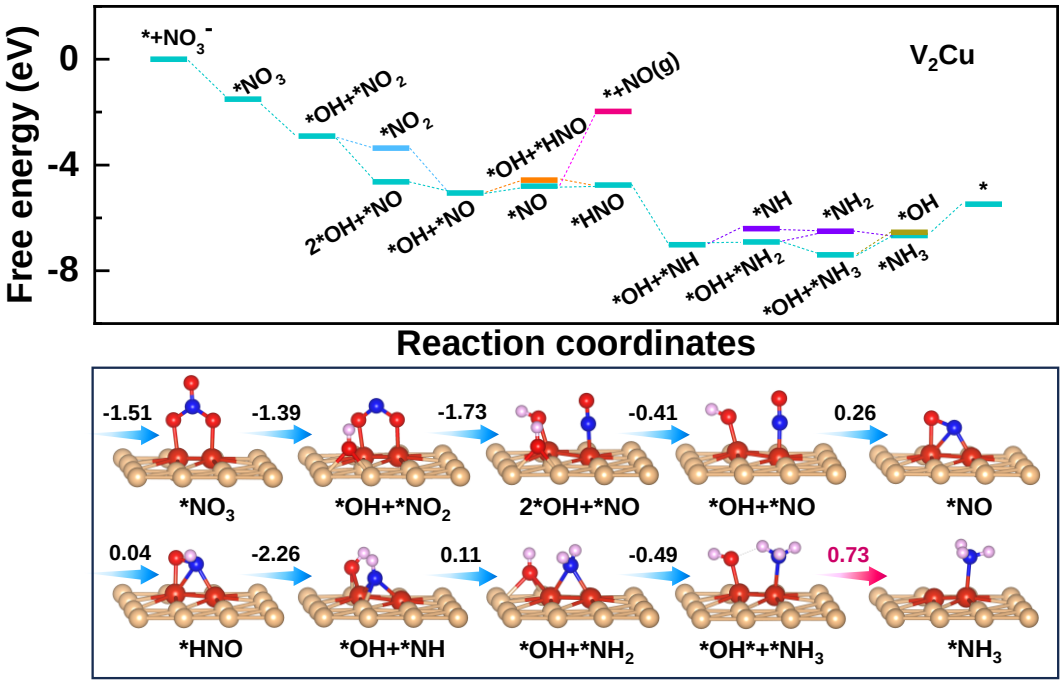

Fig. S10. Free energy diagram and the configurations of corresponding intermediates for the eNO_3RR on V_2Cu.

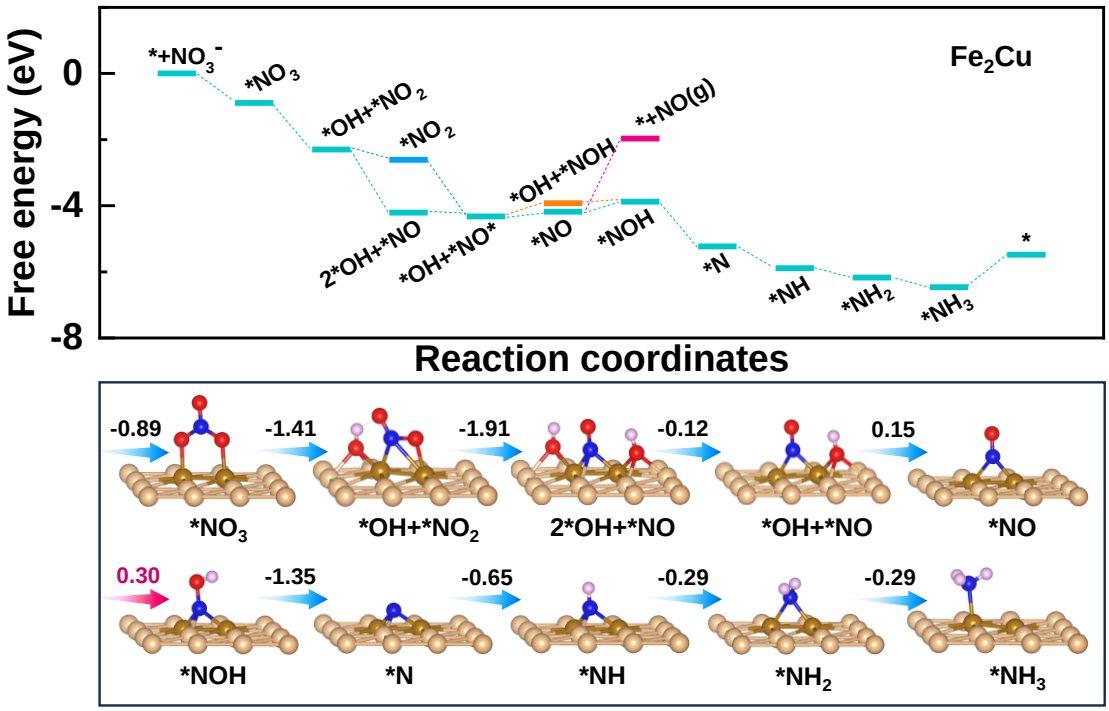

Fig. S11. Free energy diagram and the configurations of corresponding intermediates for the eNO_3RR on Fe_2Cu.

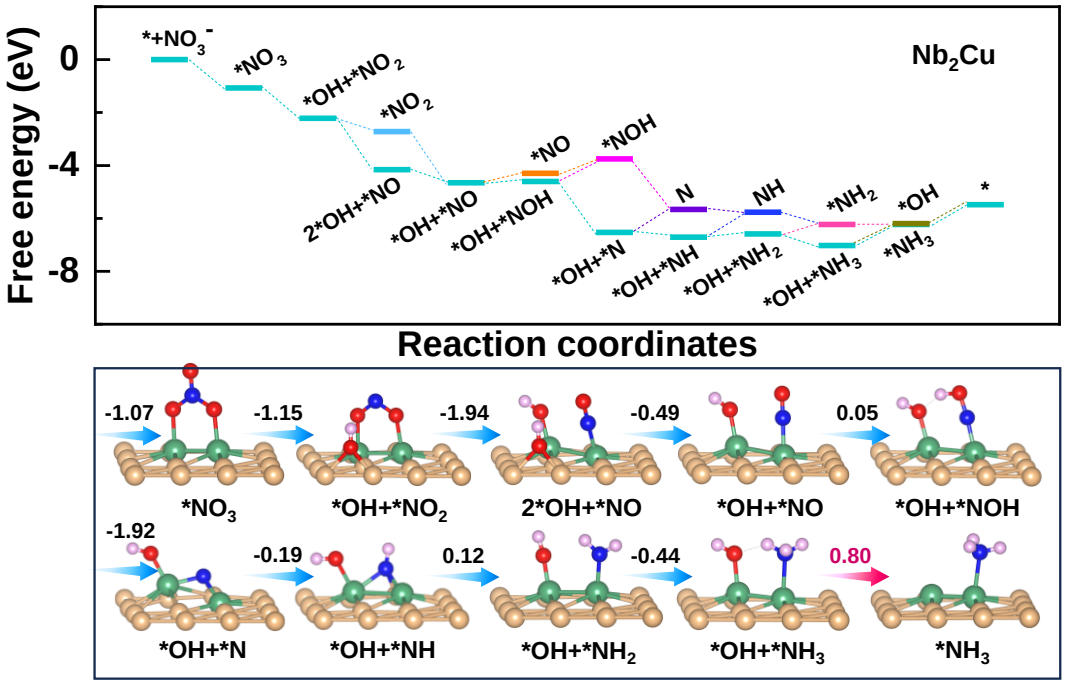

Fig. S12. Free energy diagram and the configurations of corresponding intermediates for the eNO_3RR on Nb_2Cu.

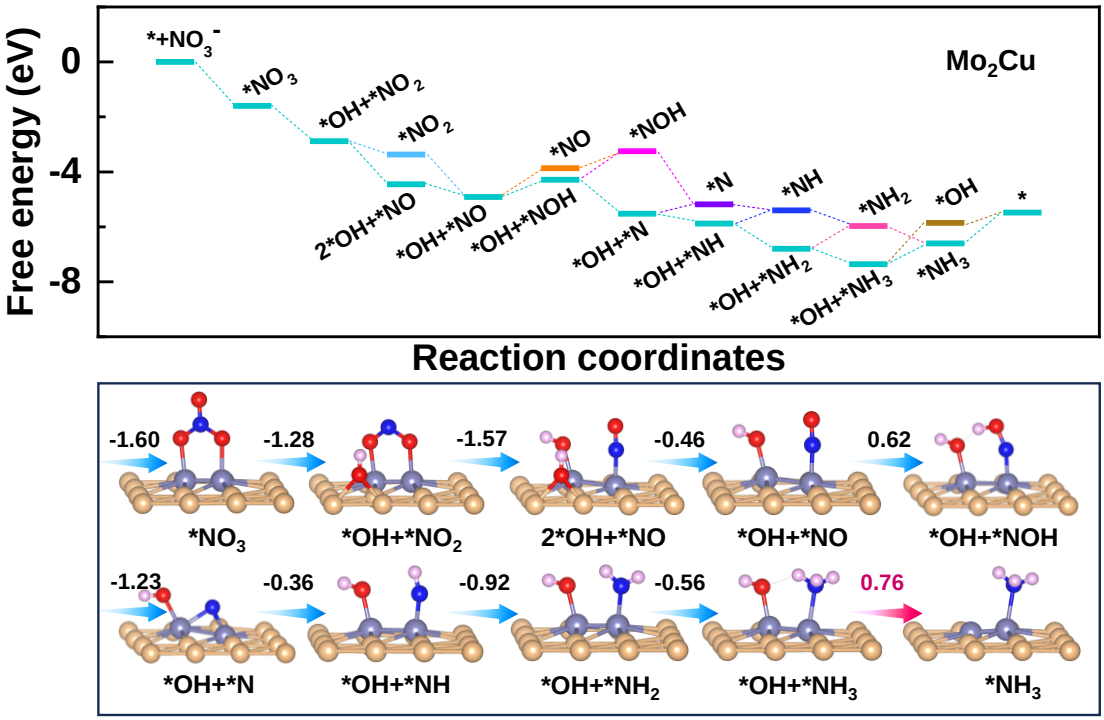

Fig. S13. Free energy diagram and the configurations of corresponding intermediates for the eNO_3RR on Mo_2Cu.

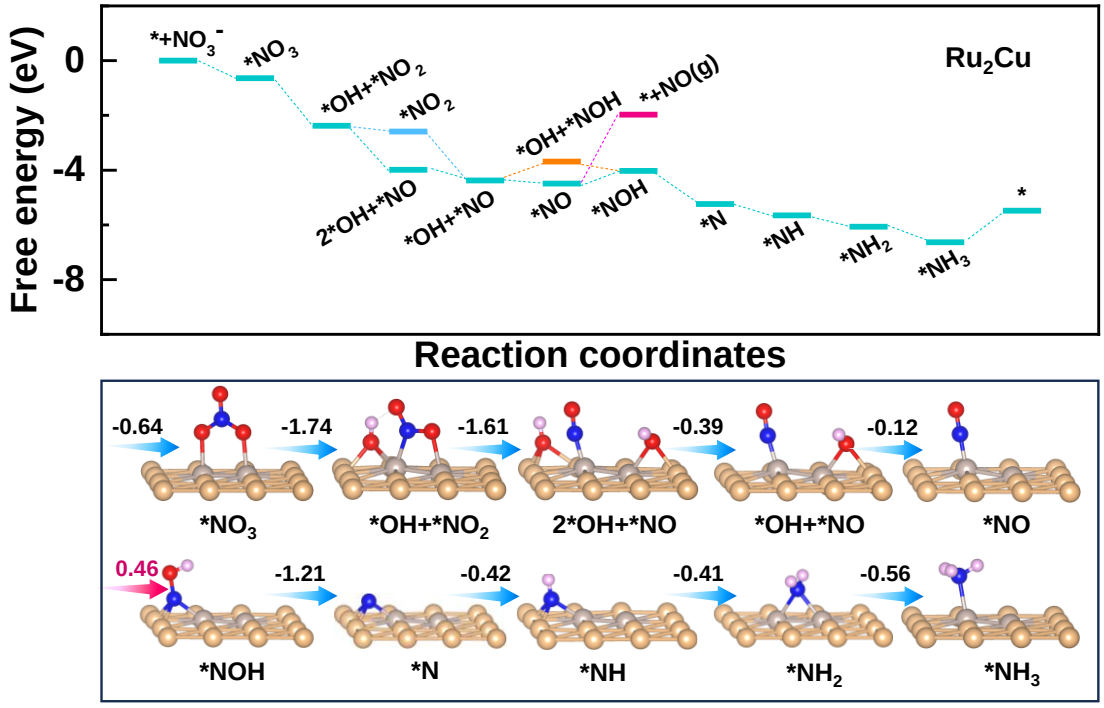

Fig. S14. Free energy diagram and the configurations of corresponding intermediates for the eNO_3RR on Ru_2Cu.

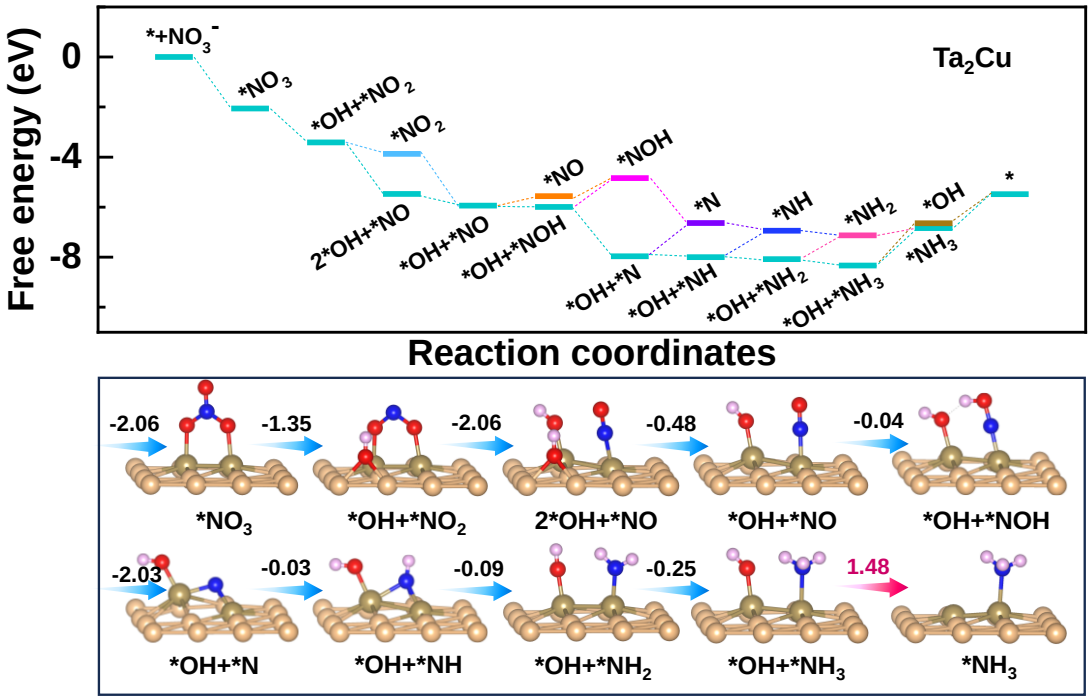

Fig. S15. Free energy diagram and the configurations of corresponding intermediates for the eNO$_3$RR on Ta$_2$Cu.

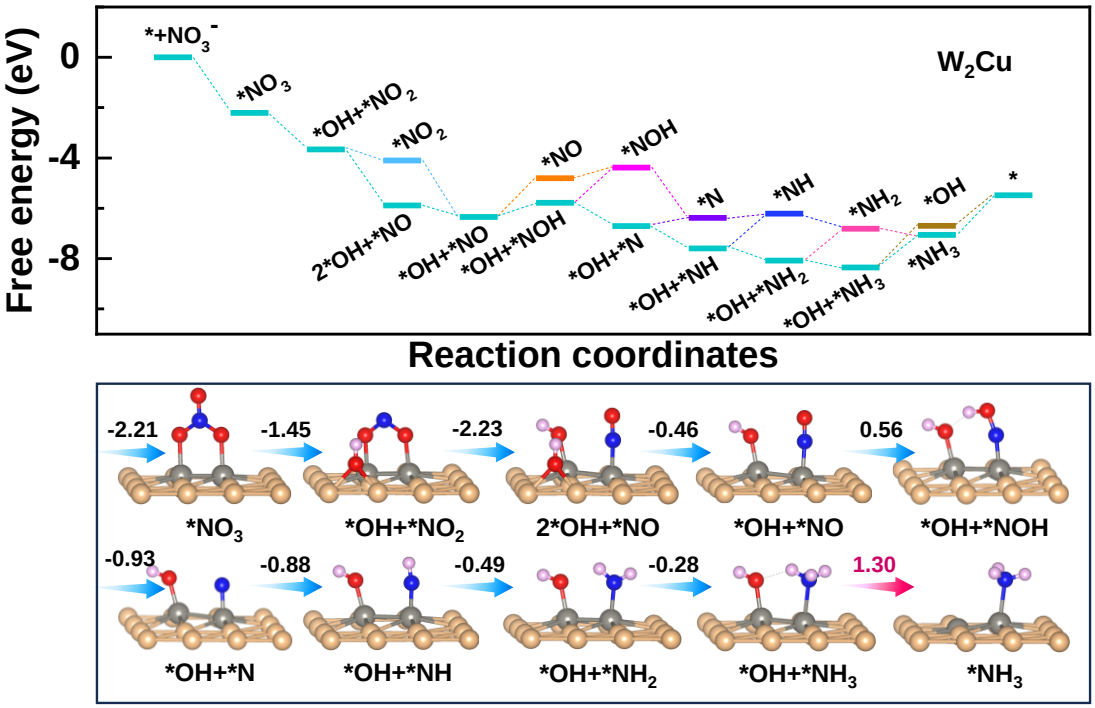

Fig. S16. Free energy diagram and the configurations of corresponding intermediates for the eNO$_3$RR on W_2Cu.

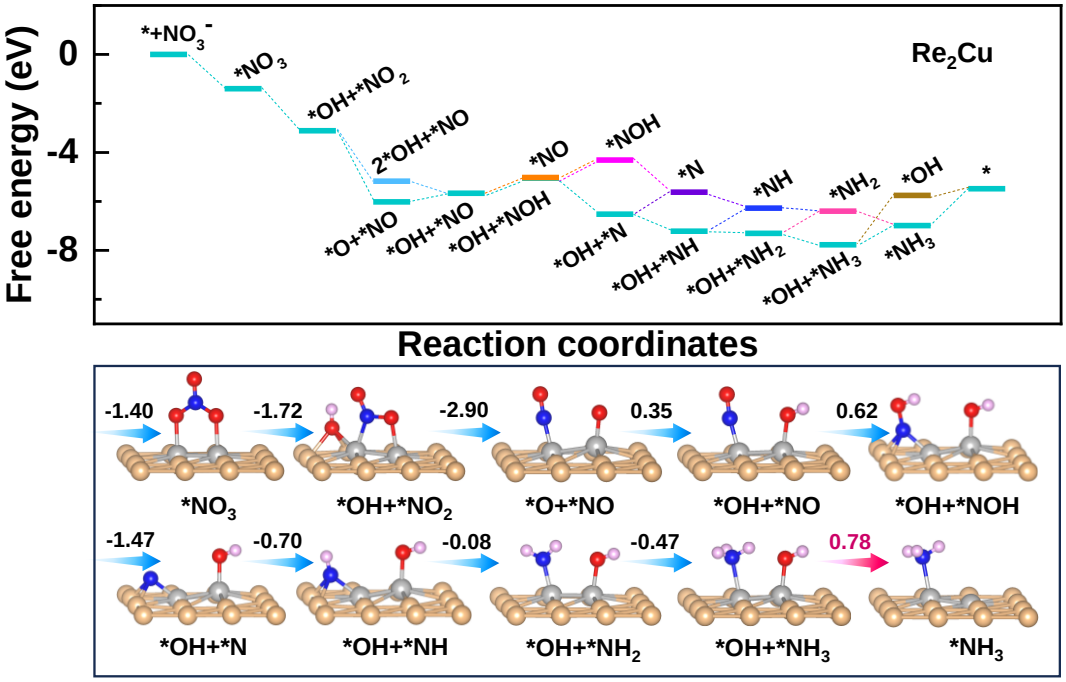

Fig. S17. Free energy diagram and the configurations of corresponding intermediates for the eNO_3RR on Re_2Cu.

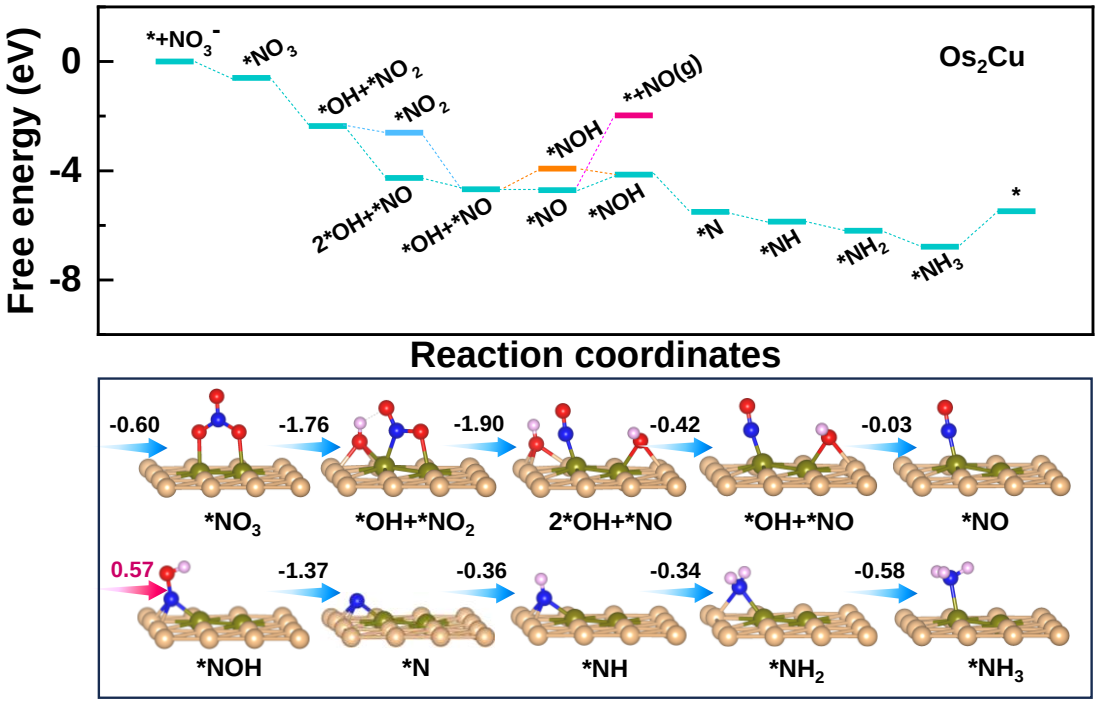

Fig. S18. Free energy diagram and the configurations of corresponding intermediates for the eNO_3RR on Os_2Cu.

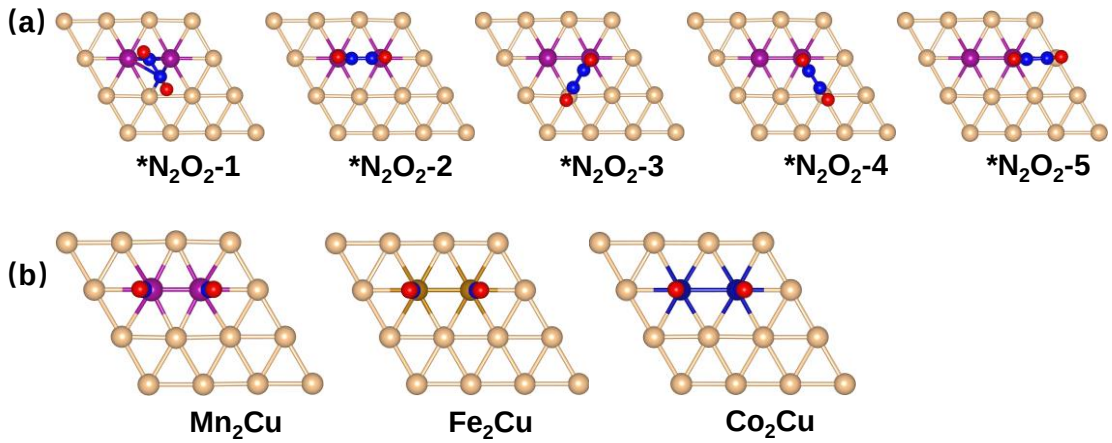

Fig. S19. (a) The considered adsorption sites and initial configurations of $*N_2O_2$ on TM_2Cu. (b)The most stable adsorption configuration of $*N_2O_2$ on Mn_2Cu, Fe_2Cu and Co_2Cu.

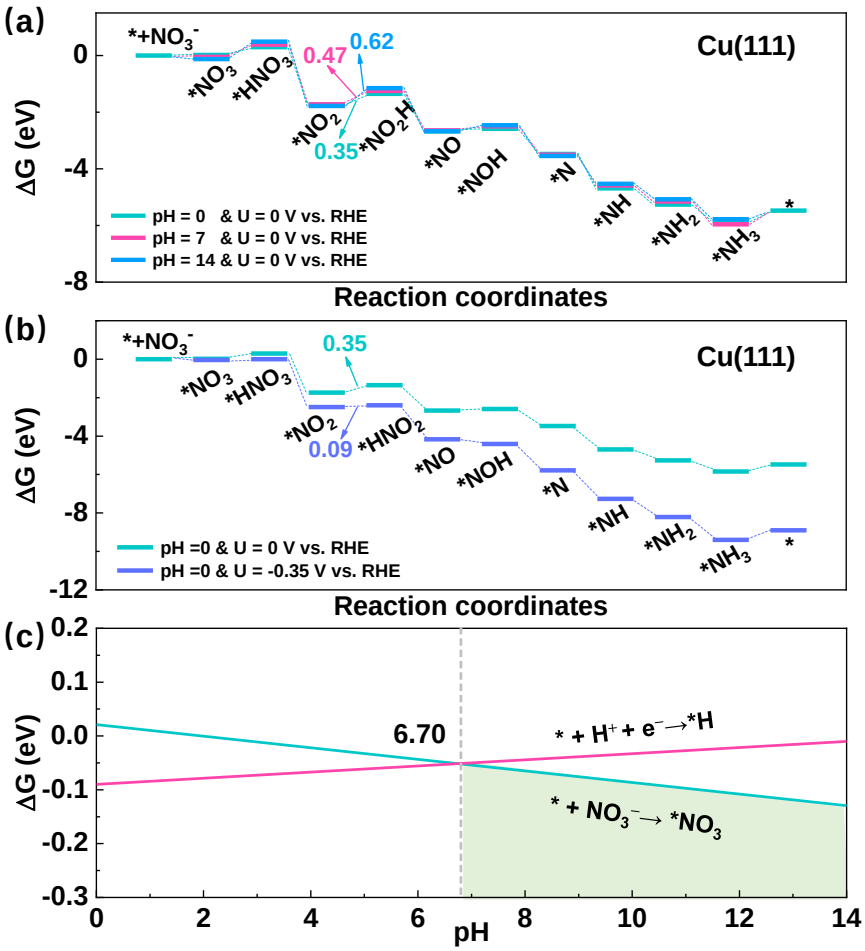

Fig. S20. (a) eNO_3RR free energy diagram along the optimal reaction path at different pH conditions for Cu(111). (b) eNO_3RR free energy diagram along the optimal reaction path at applied potentials for Cu(111). (c) The competitive relationship of $\Delta G(*NO_3)$ and $\Delta G(*H)$ between eNO_3RR and HER in all pH region on Cu(111).

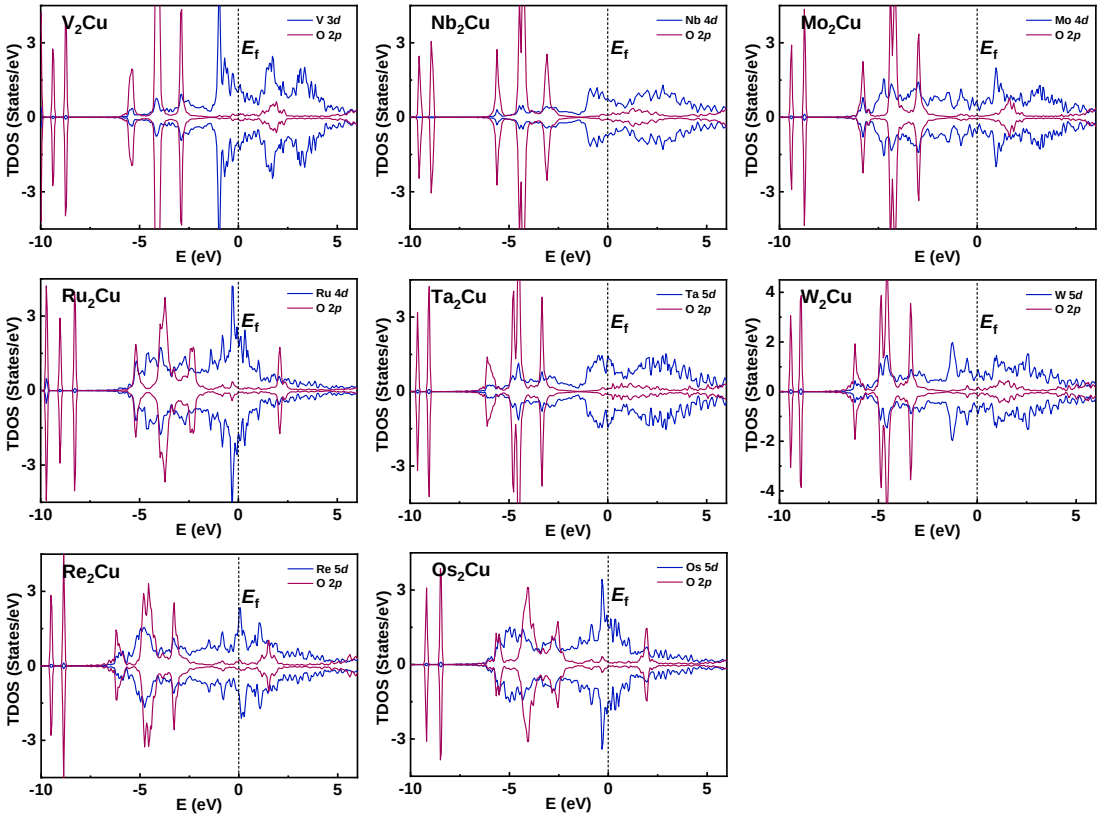

Fig. S21. Projected densities of states (PDOS) of the TM and O (in *NO_3) 2*p* states, which is bonded with the TM atom. The vertical dashed line denotes the position of Fermi level (E_f).

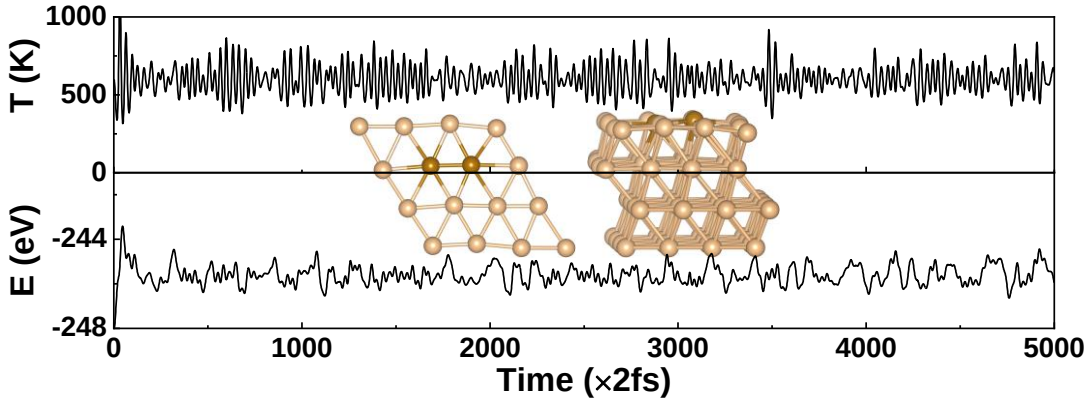

Fig. S22. The changes of temperature and energy during the AIMD simulation lasting 20 ps for Fe_2Cu, the top and side view of final configurations for the AIMD simulation are displayed.